Effect of alloying in monolayer niobium dichalcogenide superconductors

Darshana Wickramaratne
Center for Computational Materials Science, U.S. Naval Research Laboratory, Washington, DC 20375, USA

I.I. Mazin
Department of Physics and Astronomy, George Mason University, Fairfax, VA 22030, USA and
Quantum Science and Engineering Center, George Mason University, Fairfax, VA 22030, USA

(Dated: January 8, 2022)

When sulfur and silicon are incorporated in monolayer 2H-$NbSe_2$ the superconducting transition temperature has been found to vary non-monotonically. This was assumed to be a manifestation of fractal superconductivity. However, several key questions about this result are not known: (1) Does the electronic structure of $NbSe_2$ in the presence of sulfur and silicon differ from the parent compounds, (2) Are spin fluctuations which have been shown to be prominent in monolayer $NbSe_2$ also present in the alloys? Using first-principles calculations, we present a framework that provides a complete explanation for this non-monotonic change of T_c. A unifying aspect are selenium vacancies in $NbSe_2$, which are magnetic pair-breaking defects that we propose can be present in considerable concentrations in as-grown $NbSe_2$. We show that both sulfur and silicon can occupy the selenium sites and reduce the pair-breaking effect. Furthermore, when sulfur is incorporated in to $NbSe_2$, the density of states at the Fermi level and the proximity to magnetism in are both reduced compared to the parent compound; the former would decrease the transition temperature while the latter would increase it. Based on our results, we propose an alternative explanation of the non-monotonic change in T_c when sulfur and silicon are incorporated in to $NbSe_2$, which does not require the conjecture of multifractality.

I. INTRODUCTION

Ising superconductivity in two-dimensional materials is a rapidly growing field of theoretical and experimental research [1–8]. The combination of broken-inversion symmetry and strong spin-orbit coupling present in single monolayers (MLs) of the two-dimensional transition metal dichalcogenides leads to Fermi surfaces where the spin of the electrons is perpendicular to the plane of the monolayer and the electron spin direction flips between time-reversal invariant points of the Brillouin zone. This has been experimentally confirmed by establishing, for example in $NbSe_2$, that the superconducting critical field is significantly higher in-plane versus out-of-plane, and much larger that the Pauli limit [1]. While there have been extensive phenomenological descriptions of Ising superconductivity, there are several intriguing material-specific puzzles.

In $NbSe_2$, which is the most widely studied Ising superconductor, the superconducting transition temperature, T_c, decreases from $\sim$6 K to $\sim 3-4$ K, when it is reduced from bulk to a single monolayer [1]. Similar studies conducted on NbS_2 provide an intriguing contrast. In 2H-NbS_2 T_c is $\sim$ 6 K, while superconductivity has not been observed in bulk 3R-NbS_2 [9, 10]. These two polytypes differ in the stacking of the individual monolayers, while within each ML Nb atoms are in a trigonal prismatic coordination with the chalcogen atom, similar to $NbSe_2$. Reducing the thickness of NbS_2 leads to a strong suppression in T_c [11]. Superconductivity has not been found in ML NbS_2.

It was recently reported that when ML $NbSe_2$ is alloyed with sulfur, S, the T_c increases up to a S content of x=0.4 [12] in ML NbS_xSe_{2-x} alloys. For S content greater than $\sim$ 0.4, the T_c was then found to decrease monotonically [12] exhibiting qualitatively similar behavior to the bulk alloys. A non-monotonic change in T_c was also found when silicon, Si, was deposited on the surface of the same $NbSe_2$ samples, where it was assumed that Si was adsorbed on the monolayer. Up to a Si coverage of 0.05 Si atoms per $NbSe_2$ formula unit, the T_c increased. For larger concentrations of Si, the T_c was decreased and superconductivity was completely quenched at $\sim$0.17 Si atoms per $NbSe_2$ formula unit. These non-monotonic changes in T_c due to S and Si in $NbSe_2$ was interpreted as disorder-induced enchancement of T_c which possibly arises from the multifractality of the electronic wave functions [13, 14]. Implicit in this assumption is that the effect of alloying (either with Si or S) on electronic and Coulomb interactions is sufficiently weak so as to not impact T_c directly. While this is an enticing consideration, there are several important questions and experimental puzzles that need to be addressed first, which we briefly outline.

The measurements where fractal superconductivity was observed report a T_c for ML $NbSe_2$ that is $\sim$ 2 K lower than the widely accepted T_c of ML $NbSe_2$, $\sim$3 to 4 K [1, 5]. In fact, the peak T_c where fractal superconductivity is observed is $\sim$ 3 K, which occurs for $0.2 \leq x \leq 0.5$ due to alloying with S. We also note the experimental in-plane lattice constant is relatively unchanged for $0 \leq x \leq 0.2$ [15]. If the T_c of $NbSe_2$ in Ref. [12] occurred at the more widely accepted 3 to 4 K, this would not lead to a dome-shaped dependence of T_c on S and Si content, as illustrated in Fig.1. Instead, T_c would decrease linearly with S content, as has been found when S is alloyed into

bulk $NbSe_2$ [16, 17].

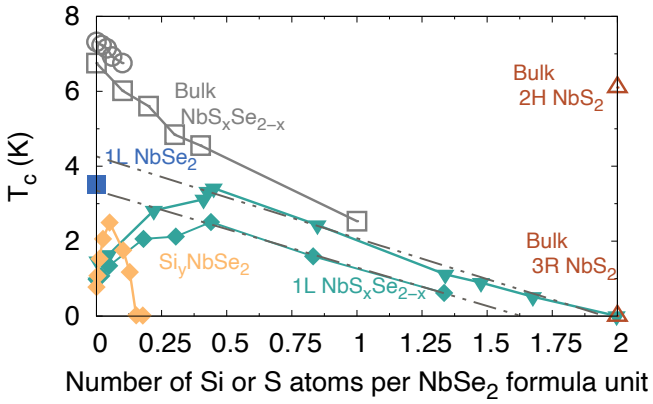

FIG. 1. Experimental reports of the superconducting transition temperature versus alloy concentration in bulk and ML NbS_xSe_{2-x} alloys as a function of S content, x and Si content, y. The references associated with each marker is as follows: □ [17], ○ [16], ▽ and ◇, [12], △ [10] and ■ [1]. Open symbols correspond to measurements on bulk samples while filled symbols correspond to measurements on ML samples. The dotted lines correspond to a linear extrapolation of the ML data for $x > 0.4$. See the main text for the discussion on the extrapolation.

Taken together, we arrive at three possible mechanisms that can lead to this non-monotonic dependence of T_c on S and Si content. The first is the role of fractal superconductivity, which was invoked in Refs. [12, 18]. While this exotic phenomenon may lead to a non-monotonic change in T_c [19], the success of this model requires information on a plethora of material-dependent parameters that are often not accessible by experiment alone. A second possible mechanism is the role of the charge-density wave (CDW), which has been shown to lead to a pseudogapping of the Fermi surface in ML $NbSe_2$ [20, 21], and thus to a reduction in T_c. However, recent studies have suggested the CDW transition temperature varies little when $NbSe_2$ transitions from bulk to a single ML [22, 23], while T_c exhibits a large change [1]. This would imply that the coupling between the superconducting and CDW order parameters is weak, as has been found in studies on bulk $NbSe_2$ [24, 25].

A third mechanism is the collective role of point defects [4] and spin fluctuations [6], both of which have been suggested as a source of pair breaking in ML $NbSe_2$. Experimental studies on ML $NbSe_2$ have found the selenium, Se, vacancy concentration can be large (equivalent to a bulk concentration of $\sim 10^{21}$ cm^{-3}), depending on the growth conditions [26]. Selenium vacancies, which are magnetic point defects in $NbSe_2$ [27], can act as a source of pair-breaking and decrease T_c. However, during the growth of NbS_xSe_{2-x} alloys, S, which is isovalent to Se, but more electronegative, can occupy the Se vacancies and lower the concentration of pair-breaking defects. This is analagous to the finding that oxygen can substitute for sulfur (both of which are isovalent) in sulfur-deficient ML TaS_2, and lead to an increase in T_c compared to ML TaS_2. [28]. Since Si and Se have approximately similar atomic radii the possibility for Si substitution for Se vacancy sites also exists.

Alloying will also lead to changes in the electronic structure, which may also affect the proximity of the material to magnetism or lead to changes in the density of states (DOS) at the Fermi level, and therefore T_c. There is *a priori* no means to determine how all of these properties change with alloying. Furthermore, if defects are indeed the source of the lower T_c in $NbSe_2$, this raises questions on the purported relationship between the non-monotonic dependence of T_c and fractal superconductivity [12].

In the present work we propose an alternative solution that reconciles these puzzles. Using first-principles density functional theory calculations (Sec. V) we show that this non-monotonic dependence of T_c on sulfur and silicon content can emerge from the interplay between defects and the effect of alloying on the electronic structure and spin-fluctuations. We show that S is completely miscible in $NbSe_2$, across the entire alloy composition range. For finite concentrations of S in NbS_xSe_{2-x} we find a reduction of the density of states at the Fermi level *and* a weakening of magnetism, compared to the parent compounds, $NbSe_2$ and NbS_2. We also show there is a minimum energy pathway that would result in Si adatoms that are deposited on $NbSe_2$ to be incorporated substitutionally on the Se site or as an interstitial. We conjecture a combination of these effects can lead to a non-monotonic dependence of T_c on S and Si content, without having to invoke the phenomenon of multifractality.

II. RESULTS

Predictions for sulfur in $NbSe_2$

We start by considering the properties of chalcogen vacancies in NbS_2 and $NbSe_2$ in the dilute limit. The formation energies of a S vacancy, V_S, in NbS_2 and a Se vacancy, V_{Se}, in $NbSe_2$ is listed in Table I.

TABLE I. Formation energy of chalcogen vacancies in $NbSe_2$ and NbS_2 under Nb-rich and Nb-poor conditions

Defect	Nb-rich (eV)	Nb-poor (eV)
V_{Se}	0.7	1.7
V_S	1.2	2

The results show that the formation energy of V_{Se} is lower than V_S, even under Se-rich conditions that were used in the growth of the $NbSe_2$ samples in Ref. [12]. This suggests that as-grown ML $NbSe_2$ is likely to have a higher concentration of Se vacancies compared to S vacancies in NbS_2. We also considered the possibility that S may substitute on the Nb site and calculated the

formation energy of this defect, S_{Nb}, in ML $NbSe_2$. In the dilute limit we find the formation energy of S_{Nb} to be larger than the formation energy of V_{Se}. Hence, for the purposes of alloying beyond the dilute limit we only consider substitution of S on the Se site.

Next we check the stability of NbS_xSe_{2-x} alloys with respect to decomposing into their parent compounds, $NbSe_2$ and NbS_2. Figure 2 illustrates the lowest enthalpy structure for each composition. We find the T= 0 K formation enthalpy across the entire range of compositions is negative which suggests ordered NbS_xSe_{2-x} alloys are stable with respect to decomposition into the parent compounds.

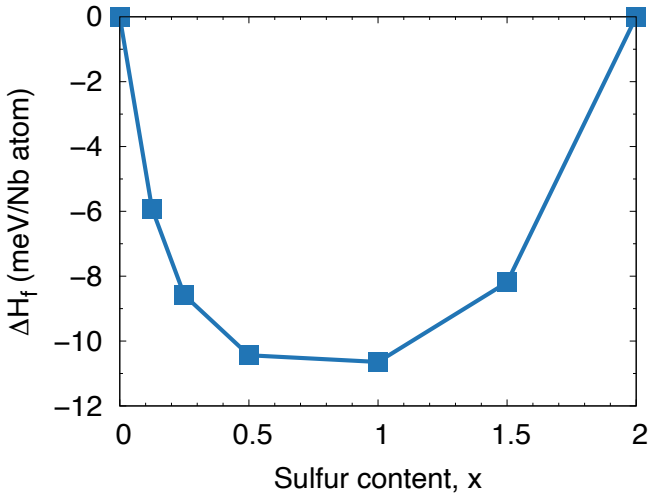

FIG. 2. Formation enthalpy as a function of S content, x, in NbS_xSe_{2-x}

We now turn to the electronic and magnetic properties of the alloys. We first consider the parent compounds, $NbSe_2$ and NbS_2. In a single ML the Nb atoms are in a trigonal prismatic coordination with the chalcogen atoms. In ML $NbSe_2$ the trigonal crystal field that acts on the 4d states of Nb^{4+} leads to one band that crosses the Fermi level, which generates Fermi contours at Γ, K and K′ [6]. The combination of broken inversion symmetry in the monolayer and strong spin-orbit coupling leads to a spin-orbit splitting of the spin degenerate band along the M-K-Γ line of the Brillouin zone. Since the 4d states of Nb^{4+} in NbS_2 are also in a trigonal prismatic coordination, albeit with a shorter Nb-S bond length compared to the Nb-Se bond length, the qualitative features of the band structure between the two materials are similar [15].

ML $NbSe_2$ exhibits strong spin fluctuations, which have been highlighted as a potential source of pair breaking [6, 29–31]. First-principles calculations have shown that monolayer $NbSe_2$ can host ferromagnetic spin fluctuations with a sizeable Stoner renormalization, and an antiferromagnetic spin spiral state with **q** vector (0.2,0,0) [6, 30]. In ML $NbSe_2$ we find the spin spiral state to be 1.7 meV/Nb atom lower in energy compared to the nonmagnetic state. In NbS_2, we find a spin spiral state at a **q**-vector of (0.2,0,0) is also stable [15] and is is 1.9 meV/Nb atom lower in energy compared to the nonmagnetic ground state. If spin fluctuations are sizeable in the alloy they can impact pairing interactions.

To study the effect of alloying on the spin spiral energies we use virtual crystal approximation (VCA) calculations (Sec. V) for S contents that correspond to x=0.5, 1 and 1.5. Figure 3(a) illustrates the energy difference between the spin spiral state with respect to the nonmagnetic state, $\Delta E_{\rm spiral}$, in NbS_xSe_{2-x} When S is alloyed into $NbSe_2$, the spin spiral state is less stable for intermediate values of S content than for either $NbSe_2$ and NbS_2. At x=1 we find $\Delta E_{\rm spiral}$ decreases by a factor of 2.1 compared to NbS_2 where the magnitude of $\Delta E_{\rm spiral}$ is the largest. The magnitude of the magnetic moment on the Nb atom is also suppressed by up to $\simeq$ 25% in the spin-spiral state for the alloys with finite S content compared to the parent compounds, as illustrated in Fig. 3(a).

Next we consider whether ferromagnetic spin fluctuations, which are present in $NbSe_2$, are also impacted due to alloying by using the VCA and collinear fixed-spin moment calculations for ML $NbSe_2$, NbS_2, NbSSe, $NbS_{1.5}Se_{0.5}$, and $NbS_{0.5}Se_{1.5}$. The quantity of interest is the ferromagnetic spin susceptibility, χ, which is defined as $\chi = a_1^{-1} = \left(\frac{\delta^2 E}{\delta m^2}\right)^{-1}$ (see Methods). We find χ varies non-monotonically as a function of S content as illustrated in the inset of Fig. 3(b), where it is large for $NbSe_2$ and NbS_2 and suppressed in the case of the alloys. Hence, it is reasonable to assume that the spin fluctuations for intermediate concentrations are supressed non-monotonically for all relevant wave vectors. In both cases these fluctuations are the weakest at roughly equal concentrations of S and Se.

The origin of the reduction in χ (and, probably, also $\Delta E_{\rm spiral}$, given the relatively small spiral vector of (0.2,0,0)) can be understood by examining the density of states (DOS). The DOS at the Fermi level, $N(\mathrm{E_F})$ as a function of S content is illustrated in Fig. 3(c). In $NbSe_2$ and NbS_2, $N(E_F)$ is suppressed from 2.8 states/eV/Nb atom in the nonmagnetic structure to 2.14 states/eV/Nb atom in $NbSe_2$ and 2.18 states/eV/Nb atom in NbS_2 in the spin spiral ground state [15]). We also find $N(E_F)$ is suppressed for the alloys at x=0.5,1, and 1.5, where in the non-magnetic state $N(E_F)$ is ∼2.5 states/eV/Nb atom while in the spin spiral state it reduces to 1.9 states/eV/Nb atom. Hence, for the parent compounds and the alloys, our calculations indicate there is a gain in one-electron energy by transitioning to the spin spiral state. We also find that in the spin spiral state, the magnitude of $N(E_F)$ of the alloys decreases by 10% compared to $N(E_F)$ of the parent compounds. Such a small change in $N(E_F)$ as a function of S content is consistent with the fact that $N(E_F)$ is comprised almost entirely of Nb d-states in $NbSe_2$ and NbS_2.

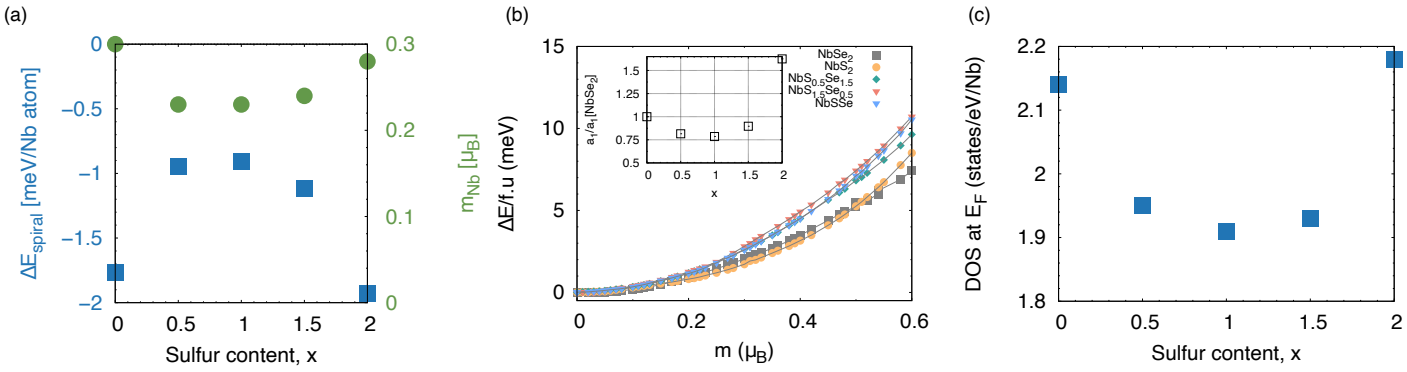

FIG. 3. (a) Energy difference between the spin spiral state and the non magnetic state as a function of sulfur content, x, in NbS_xSe_{2-x} (blue, left vertical axis – ■). Magnetic moment per Nb atom as a function of sulfur content in the spin spiral calculation with finite q (green, right vertical axis – ○). (b) Collinear fixed-spin moment calculations of $NbSe_2$ (grey - ■), NbS_2 (orange - ○), $NbS_{0.5}Se_{1.5}$ (teal - ◇), NbSSe (red - ▽), and $NbS_{1.5}Se_{0.5}$ (blue - △) illustrate the change in energy per formula unit with respect to the non-magnetic state as a function of magnetic moment per Nb atom. The inset illustrates the coefficient a_1 (see main text) normalized by the value of a_1 in $NbSe_2$. (c) Density of states at the Fermi level, E_F, as a function of sulfur content, x. The magnitude of the DOS for $NbSe_2$ and NbS_2 correspond to the spin spiral state [15].

Predictions for silicon in $NbSe_2$

We now present our results for the properties of Si in monolayer $NbSe_2$. The formation energies for Si incorporated substitutionally (on the Nb site, Si_{Nb} and on the Se site, Si_{Se}), adsorbed at high-symmetry positions on top of the $NbSe_2$ monolayer, Si_{ads} (where we consider the hollow site formed by the triangle of Se atoms, Si_{ads}^{hollow}, and vertically above either a Se atom, Si_{ads}^{Se}, or Nb atom, Si_{ads}^{Nb}) and Si incorporated interstitially, Se_i, is summarized in Table II.

TABLE II. Formation energy of Si in $NbSe_2$ under Nb-rich conditions. Results are for Si substituting on the Nb site, Si_{Nb}, Si substituting on the Se site, Si_{Se}, Si adsorbed above the hollow site, Si_{ads}^{hollow}, Si adsorbed vertically above a Se atom, Si_{ads}^{Se}, Si adsorbed vertically above a niobium site, Si_{ads}^{Nb}, and and Si incorporated interstitially, Si_i, in monolayer $NbSe_2$

Defect	Formation energy (eV)
Si_{Nb}	3.04
Si_{Se}	1.26
Si_i	1.59
Si_{ads}^{hollow}	1.14
Si_{ads}^{Se}	3.06
Si_{ads}^{Nb}	0.49

If Si is deposited on the $NbSe_2$ surface we find that it is likely to initially adsorb on the Si_{ads}^{Nb} site, *not* the Si_{ads}^{Se} site (which was implicitly assumed to be the most stable configuration for Si in Ref. [12]). The likelihood of Si remaining adsorbed on the $NbSe_2$ surface is determined in part by the migration barrier of Si adatoms. We calculated the minimum energy pathway for a Si adatom to migrate from the metastable site, Si_{ads}^{Se}, to the Si_{ads}^{Nb} adsorption site and find it to be barrier-less as illustrated in Fig. 4(a). Subsequent hops between Si_{ads}^{Nb} sites occurs with a low migration barrier of 0.11 eV, which would render Si adatoms to be highly mobile even at low temperatures.

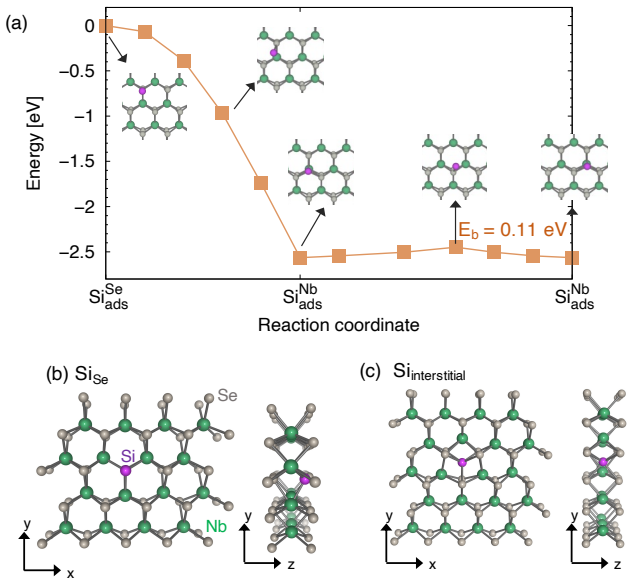

FIG. 4. (a) Theoretical minimum-energy pathway for Si adatoms on $NbSe_2$ to migrate from the Si_{ads}^{Se} metastable adsorption site to Si_{ads}^{Nb}. The migration barrier to hop between Si_{ads}^{Nb} sites is 0.11 eV. The energies are reported with respect to the total energy of Si_{ads}^{Se}. Schematic top view and side view of (b) Si substituted on the Se site, Si_{Se} and (c) Si incorporated interstitially within the same plane as the the Nb atoms, Si_i.

The low migration barrier of Si on the surface of $NbSe_2$. makes it unlikely that Si adatoms will exist as isolated defects. Our formation energy calculations suggest that Si adatoms will likely be incorporated as Si_{Se} or as Si_i,

which are the two lowest energy configurations for Si that is not adsorbed on $NbSe_2$. If there is a large concentration of Se vacancies, as we suggest are present in Ref. [12], Si that is deposited on $NbSe_2$ will migrate and substitute for the Se sites when it encounters a V_{Se}. The STM images of Si deposited on $NbSe_2$ (cf. Fig. S9a in Ref. [12]) provides us a clue that supports this assertion. The STM images show bright spots associated with Si residing at Se sites. Our formation energy calculations in Table II show that it is unlikely for Si to adsorbed above Se. Hence, the experiments in Ref. [12] unambiguously shows that Si atoms indeed substitute for Se. When Si substitutes for Se as illustrated in Fig. 4(b), Si is bonded to three nearest-neighbor Nb atoms with a Si-Nb bond length of 2.615 Å, which is 4.5% shorter than the equilibrium Nb-Se bond length.

For higher concentrations of Si, once all of the Se vacancy sites are occupied we expect Si to incorporate as an interstitial where it sits in the same plane as the Nb atoms. In this configuration, Si_i displaces one of the Nb atoms that it is adjacent to and is six-fold coordinated by the Se atoms with a Si-Se bond length of ∼2.60 Å , which is illustrated in Fig. 4(c).

III. DISCUSSION

Here we propose a framework to understand how this seemingly diverse set of results on Si and S in $NbSe_2$ can be used to understand the non-monotonic change of T_c in $NbSe_2$ observed in Ref. [12], without invoking multifractality. Since the formation energy of Se vacancies in $NbSe_2$ is low, Se vacancies are likely to exist in considerable concentration in as-grown $NbSe_2$, which is consistent with experimental observations. We have previously shown, using first-principles calculations, that V_{Se} in $NbSe_2$ is a magnetic point defect that results in a finite magnetization of $\sim 0.6\ \mu_B$ [27]. This finite magnetization spans a length scale of up to 15Å and is likely to have an easy axis along $\hat{z}$. Hence, in the Ising superconductor $NbSe_2$ they will be pair-breaking [27] and suppress T_c, as in a regular s-wave superconductor [32]. This is consistent with measurements on ML $NbSe_2$, where low values of T_c are found in samples where the residual resistivity ratio is low [26]. Our calculations show that the substitution of S on the Se site in $NbSe_2$ is energetically favorable for all S compositions. Hence, during the growth of NbS_xSe_{2-x} we expect S to occupy the sites of missing Se atoms up to a critical S composition. This would lower the concentration of pair-breaking V_{Se} defects and lead to an increase in T_c. This immediately explains why the putative multifractal behavior was observed in $NbSe_2$ samples with suppressed T_c, compared to the samples in the literature with lower defect concentrations, which is correlated with higher T_c.

We also anticipate the presence of Se vacancies to play a key role when Si is deposited on $NbSe_2$ [12]. The low migration barrier that we calculate for Si adatoms implies that the Si adatoms that are initially adsorbed vertically above the Nb site will migrate and occupy V_{Se} or Si_i sites. As V_{Se} sites are occupied by Si, the pair-breaking effect of V_{Se} will decrease and we expect T_c to increase as was indeed observed in Ref. [12] until all of the V_{Se} sites are occupied. In the experiments in Ref.[12] we expect this to occur up to a Si coverage of $\sim$ 0.05 Si atoms per $NbSe_2$ formula unit, which is where the peak T_c in the $NbSe_2$ samples with Si occurs (Fig. 1). Beyond this concentration, we expect the Si atoms to incorporate interstitially within the $NbSe_2$ lattice as illustrated in Fig. 4(c).

While the increase in T_c in the $NbSe_2$ samples with S and Si can be understood by considering the role of V_{Se} the subsequent reduction in T_c at higher concentrations of S and Si can have different origins. One possible consideration is the role of ionized impurity scattering. However, experimentally, there is no indication of ionized impurity scattering in the NbS_xSe_{2-x} alloys since T_c decreases monotonically for $x \geq 0.4$ (Fig. 1) and does not exhibit any convex variations of T_c with x.

We also find that both $NbSe_2$ and NbS_2 host strong spin fluctuations at all wave vectors. First-principles calculations on monolayer $NbSe_2$ suggest that spin fluctuations play a role in suppressing T_c when compared to the T_c obtained by electron-phonon coupling alone [33]. However, for finite S compositions in NbS_xSe_{2-x} this tendency towards magnetism is weakened, which favors superconductivity. This reduction in the proximity to magnetism competes with a reduction in $N(E_F)$ of the alloys compared to $NbSe_2$ and NbS_2, which would decrease the electron-phonon coupling constant, λ_{ep}, and weaken superconductivity. We can estimate the sign of the net effect using the general expression derived in Ref. [34], under a simplifying assumption that the spin-fluctuations and phonons have comparable frequencies. Then $d\log T_c/d\log\lambda_{ep} \propto \lambda_{ep} + 2\lambda_{ep}\lambda_{sf}$, and $-d\log T_c/d\log\lambda_{sf} \propto \lambda_{sf} + 2\lambda_{sf}\lambda_{ep}$. The DOS is reduced by $\approx$ 10% between the end composition and the midpoint. In contrast, the tendency to magnetism, as measured by the spin-spiral energy gain, decreases by a factor of 2, between the end composition and the midpoint. The latter is expected to be more important, at least for low concentrations of S. We note that the maximum T_c measured in the $NbS_xSe_{(2-x)}$ alloys [12] occurs at x=0.5 while in our calculations $N(E_F)$ and the proximity to magnetism are minimum at x=1. We anticipate that this difference is related to the complete suppression of superconductivity in monolayer NbS_2 despite $N(E_F)$ and its magnetic properties being similar to monolayer $NbSe_2$. This is an intriguing research question that deserves a more elaborate study, that is beyond the scope of this paper. We emphasize, that the goal of this paper is not to provide a quantitative prediction of T_c as a function of sulfur content, but to provide a physically intuitive explanation for the non-monotonic change in T_c that occurs in the $NbS_xSe_{(2-x)}$ alloys at low sulfur content.

Silicon incorporation in $NbSe_2$ leads to a more pro-

nounced suppression of T_c compared to S. This suppression is unlikely to be due to ionized impurity scattering as evidenced by the linear change in T_c with Si content. We suggest Si incorporated interstitially leads to doping of $NbSe_2$ that decreases T_c.

Taken together, these properties of S and Si in $NbSe_2$ collectively imply that the non-monotonic dependence of T_c on S and Si content[12] is not sufficient proof of fractal superconductivity, but likely has a rather prosaic origin: it is S or Si occupying a high concentration of Se vacancy sites (thus decreasing the concentration of pair-breaking defects). For the case of alloying with S this is also accompanied by a strong reduction of the tendency to magnetism as the S concentration increases from 0 to ~ 0.5. This effect overlaps with the general weaking of the electron-phonon matrix elements, as evidenced by the smaller coupling constant in NbS_2 compared to $NbSe_2$, despite their similar $N(E_F)$.[33, 35, 36] For the case of Si in $NbSe_2$ we expect that when Si is employed interstitially once all of the V_{Se} sites are occupied, Si_i will act as a source of doping and decrease T_c.

We have discussed two possible mechanisms that can lead to an increase in T_c when S or Si is incorporated in $NbSe_2$; (i) the presence of Se vacancies that are pair-breaking defects and (ii) a reduction in the tendency to magnetism when $NbSe_2$ is alloyed with S. Of these two mechanisms we suggest the presence of Se vacancies is likely playing a larger role. If the concentration of Se vacancies were reduced their pair-breaking effect would be suppressed. This would lead to a higher value of T_c at x=0 and the non-monotonicity that was observed would be less pronounced. Indeed, if we linearly extrapolate the $T_c(x)$ data for $x \geq 0.4$ to $x = 0$, in the $NbSe_2$ samples alloyed with S we get a T_c of $NbSe_2$ that ranges from 3.35 K to 4.2 K, as illustrated in Fig. 1. We find a similar T_c of $\sim$4 K for $NbSe_2$ if we linearly extrapolate the T_c for $y \geq 0.05$ for the $NbSe_2$ samples with Si. Furthermore, this is consistent with optimizing growth conditions, which leads to a suppression in the concentration of selenium vacancies, which in turn leads to higher values of T_c in monolayer $NbSe_2$ [37].

IV. CONCLUSIONS

In conclusion, we have presented a detailed analysis of the properties of NbS_xSe_{2-x} alloys and silicon in $NbSe_2$ using first-principles calculations. Our results, when analyzed in the context of recent studies that have asserted the presence of fractal superconductivity when S and Si are incorporated in $NbSe_2$ [12, 18], suggest multifractality isn't the only mechanism that can lead to non-monotonic changes in T_c. The following key factors emerge from our calculations: (1) the low formation energy of Se vacancies that are magnetic pair-breaking point defects, (2) the stability of NbS_xSe_{2-x} alloys across the entire composition range with respect to decomposition into the parent compounds, (3) the low migration barrier for Si adatoms on $NbSe_2$ and the low formation energy for Si substitution on the Se site in $NbSe_2$, (4) the reduction in the density of states at the Fermi level as a function of alloy content in NbS_xSe_{2-x} and (5) a reduction in the proximity to magnetism in NbS_xSe_{2-x} alloys compared to $NbSe_2$ and NbS_2.

These results suggest that as-grown $NbSe_2$ hosts a large concentration of pair-breaking Se vacancies that upon alloying are occupied by sulfur or silicon atoms. This leads to an increase in T_c up to a critical composition where the concentration of sulfur or silicon is equal to the concentration of Se vacancies that are present during the growth. For the case of alloying with sulfur, T_c monotonically decreases once sulfur occupies all of the Se vacancy sites, reflecting a general weakening of the electron-phonon matrix elements toward NbS_2. For high concentrations of silicon in $NbSe_2$ we find silicon is also likely to incorporate interstitially, where it would act as a dopant and lead to a reduction in T_c. These two distinct regimes ma[redacted] in a non-monotonic change in T_c. If the concentration of pair-breaking selenium vacancies were lower in Ref. [12] where fractal superconductivity was invoked, we expect the T_c to be higher and the non-monotonic change in the T_c to be less pronounced. Given that disorder-induced non-monotonic changes in T_c have been observed in other transition metal dichalcogenide alloys due to isovalent substitution [38–40], we expect our findings to open new avenues for investigation in this broad class of materials.

V. METHODS

Our calculations are based on density functional theory within the projector-augmented wave method [41] as implemented in the VASP code [42, 43] using the generalized gradient approximation defined by the Perdew-Burke-Ernzerhof (PBE) functional [44]. We found it is essential that Nb $5s^1, 4s^2, 4p^6, 4d^4$ electrons and Se $4s^2, 4p^4$ electrons are treated as valence. All calculations use a plane-wave energy cutoff of 400 eV. We use a $(18\times18\times1)$ Γ-centered k-point grid for the monolayer structure when performing structural optimization and calculating the electronic structure. The cell shape and atomic positions of each structure was optimized using a force convergence criteria of 5 meV/Å. All of the structures were optimized in the non-magnetic state. We verified that optimizing the structures in the spin spiral state leads to minor differences in the lattice parameters.

For the calculations of chalcogen vacancies we use a $(10\times10\times1)$ supercell of ML $NbSe_2$ and $NbSe_2$. To simulate a chalcogen vacancy we remove a single chalcogen atom (S atom in NbS_2 and Se atom in $NbSe_2$), relax all of the atomic coordinates and determine the total energy. The formation energy, of for example, a Se vacancy, V_{Se} in $NbSe_2$ is defined as:

$$E^f(V_{Se}) = E_{tot}(V_{Se}) - E_{tot}(NbSe_2) - \mu_{Se} \qquad (1)$$

where $E^f(V_{\rm Se})$ is the formation energy of the Se vacancy, $E_{\rm tot}(V_{\rm Se})$ is the total energy of the $NbSe_2$ defect supercell with a Se vacancy, $E_{\rm tot}(NbSe_2)$ is the total energy of the pristine $NbSe_2$ supercell, and $\mu_{\rm Se}$ is the chemical potential of Se. For the calculation of Si in $NbSe_2$ we use an orthorhombic supercell with 64 $NbSe_2$ formula units. We use the formation enthalpy of $SiSe_2$ as the limiting phase for our formation energy calculations of Si in $NbSe_2$. All of the defect calculations were performed with a (3×3×1) k-point grid. The theoretical minimum energy pathway for adatom migration on $NbSe_2$ was calculated using the using the nudged elastic-band method [45].

For the calculations of the alloy properties with sulfur we consider two approaches; the virtual crystal approximation (VCA) and explicit supercell calculations using either a (4×1×1) and a (4×4×1) supercell that is constructed from the unit cell of the ML structure. For each alloy supercell we consider different arrangements of the S and Se atoms for compositions corresponding to x=0.125, 0.25, 0.5, 1, and 1.5, and relax all of the atomic positions. The k-point grid for structural relaxation of each supercell is scaled with respect to the $(18 \times 18 \times 1)$ Γ-centered k-point grid we use for calculations of the unit cell.

To determine the thermodynamics of alloy formation we calculated the formation enthalpy, $\Delta H(x)$, as a function of sulfur content, x, using the (4×4×1) supercell. $\Delta H(x)$ is defined as:

$$\Delta H(x) = E(x) - xE(\mathrm{NbS_2}) - (1 - \mathrm{x})\mathrm{E}(\mathrm{NbSe_2}) \quad (2)$$

where $E(x)$ is the total energy of the alloy supercell with sulfur content, x, $E(NbS_2)$ is the total energy of the NbS_2 supercell and $E(NbSe_2)$ is the total energy of the $NbSe_2$ supercell.

We varied the lattice parameters for each alloy configuration linearly as a function of sulfur content in accordance with Vegard's law and then relax all of the atomic coordinates. For a given sulfur content, x, the in-plane lattice constant, $a(\mathrm{NbS_xSe_{2-x}})$ was varied as $a(\mathrm{NbS_xSe_{2-x}}) = xa_{\mathrm{NbS_2}} + (2-x)a_{\mathrm{NbSe_2}}$, where $a_{\mathrm{NbS_2}}$ is the in-plane lattice parameter of bulk NbS_2 and $a_{\mathrm{NbSe_2}}$ is the in-plane lattice parameter of bulk $NbSe_2$. We verified the accuracy of Vegard's law for a subset of alloy structures by allowing the lattice parameters and atomic positions to relax. In all cases, the variation of the in-plane lattice parameters was linear [15].

To calculate the spin spiral energies we used the generalized Bloch theorem formalism [46] as implemented within VASP. We use a dense $(36 \times 36 \times 1)$ Γ-centered k-point grid for the unit cell. We determine the energy difference between the spin spiral state with respect to the non-magnetic state, $\Delta E_{\rm spiral}$, which is defined as $\Delta E_{\rm spiral} = E(\mathbf{q}) - E(\mathbf{q} = \mathbf{0})$ where $E(\mathbf{q})$ is the total energy of the unit cell with spin spiral wavevector $\mathbf{q}$ and $E(\mathbf{q} = \mathbf{0})$ is the total energy of the non-magnetic unitcell.

To determine the ferromagnetic spin susceptibility, χ we used collinear fixed-spin moment (FSM) calculations (sometimes referred to as the constrained local moments approach). In our collinear FSM calculations we constrain the magnitude of the magnetic moment on the Nb atom. Performing these calculations allows us to determine the change in energy with respect to the non-magnetic ground state as a function of the total magnetization, m. We then fit our results to an expansion of the total energy as a function of m to the following expression, $E(m) = a_0 + a_1m^2 + a_2m^4 + a_3m^6 + a_4m^8$, where $E(m)$ is the total energy for a given magnetization m, to determine the ferromagnetic spin susceptibility, χ. The spin susceptibility, χ, obtained from FSM calculations is sensitive to the choice in energy convergence threshold, and the number of magnetization values used in the fit to expansion in the total energy as a function of magnetic moment. We use an energy convergence threshold of 10^{-8} eV, and up to 50 magnetization versus energy points between 0 μ_B and 0.6 μ_B for all of the FSM calculations.

The results on the formation enthalpy of the alloys are obtained using a (4×4×1) supercell with tetrahedron smearing and a $(9 \times 9 \times 1)$ k-point grid. The spin spiral energies, fixed spin moment calculations, and the density of states of the alloys are obtained using VCA calculations for sulfur contents that correspond to x=0.5, 1, and 1.5. The VCA calculations use the same k-point grid as the unit cell calculations. The in-plane lattice parameters for the x=0.5, 1, and 1.5 VCA calculations are scaled linearly according to Vegard's law. Furthermore, we also interpolate the vertical Nb-chalcogen bond length along the c-axis for each VCA alloy calculation.

DATA AVAILABILITY

The data that supports the findings of this study are available from the corresponding author upon reasonable request.

COMPETING INTERESTS

The authors declare no competing interests.

ACKNOWLEDGEMENTS

We thank Mikhail Feigel'man and Roxana Margine for helpful discussions. D.W was supported by the Office of Naval Research (ONR) through the Naval Research Laboratory's Basic Research Program. I.I.M. was supported by ONR through grant N00014-20-1-2345. Calculations by D.W. were performed at the DoD Major Shared Resource Center at AFRL.

AUTHOR CONTRIBUTIONS

D.W and I.I.M performed the first-principles calculations, analyzed the results and wrote the paper.

[1] X. Xi, Z. Wang, W. Zhao, J.-H. Park, K. T. Law, H. Berger, L. Forró, J. Shan, and K. F. Mak, Nat. Phys. **12**, 139 (2016).
[2] J. Lu, O. Zheliuk, I. Leermakers, N. F. Yuan, U. Zeitler, K. T. Law, and J. Ye, Science **350**, 1353 (2015).
[3] B. T. Zhou, N. F. Yuan, H.-L. Jiang, and K. T. Law, Phys. Rev. B **93**, 180501 (2016).
[4] D. Möckli and M. Khodas, Phys. Rev. B **101**, 014510 (2020).
[5] C. Sergio, M. R. Sinko, D. P. Gopalan, N. Sivadas, K. L. Seyler, K. Watanabe, T. Taniguchi, A. W. Tsen, X. Xu, D. Xiao, and B. Hunt, Nat. Comm. **9**, 1427 (2018).
[6] D. Wickramaratne, S. Khmelevskyi, D. F. Agterberg, and I. Mazin, Physical Review X **10**, 041003 (2020).
[7] D. Costanzo, H. Zhang, B. A. Reddy, H. Berger, and A. F. Morpurgo, Nat. Nano **13**, 483 (2018).
[8] Y. Saito, Y. Nakamura, M. S. Bahramy, Y. Kohama, J. Ye, Y. Kasahara, Y. Nakagawa, M. Onga, M. Tokunaga, T. Nojima, *et al.*, Nat. Phys. **12**, 144 (2016).
[9] I. Guillamón, H. Suderow, S. Vieira, L. Cario, P. Diener, and P. Rodiere, Physical Rev. Lett. **101**, 166407 (2008).
[10] C. Witteveen, K. Górnicka, J. Chang, M. Månsson, T. Klimczuk, and F. O. von Rohr, Dalton Transactions **50**, 3216 (2021).
[11] R. Yan, G. Khalsa, B. T. Schaefer, A. Jarjour, S. Rouvimov, K. C. Nowack, H. G. Xing, and D. Jena, Applied Physics Express **12**, 023008 (2019).
[12] K. Zhao, H. Lin, X. Xiao, W. Huang, W. Yao, M. Yan, Y. Xing, Q. Zhang, Z.-X. Li, S. Hoshino, *et al.*, Nat. Phys. **15**, 904 (2019).
[13] M. Feigel'man, L. Ioffe, V. Kravtsov, and E. Cuevas, Annals of Physics **325**, 1390 (2010).
[14] I. Burmistrov, I. Gornyi, and A. Mirlin, Phys. Rev. Lett. **111**, 066601 (2013).
[15] See Supplemental Material at [url] for additional details.
[16] H. Luo, J. Strychalska-Nowak, J. Li, J. Tao, T. Klimczuk, and R. J. Cava, Chemistry of Materials **29**, 3704 (2017).
[17] K. Sugawara, K. Yokota, J. Takemoto, Y. Tanokura, and T. Sekine, Journal of low temperature physics **91**, 39 (1993).
[18] C. Rubio-Verdu, A. M. Garcia-Garcia, H. Ryu, D.-J. Choi, J. Zaldivar, S. Tang, B. Fan, Z.-X. Shen, S.-K. Mo, J. I. Pascual, and M. M. Ugeda, Nano Letters **20**, 5111 (2020), pMID: 32463696, https://doi.org/10.1021/acs.nanolett.0c01288.
[19] B. Sacépé, M. Feigel'man, and T. M. Klapwijk, Nature Physics **16**, 734 (2020).
[20] M. Calandra, I. Mazin, and F. Mauri, Phys. Rev. B **80**, 241108 (2009).
[21] C.-S. Lian, C. Si, and W. Duan, Nano Lett. **18**, 2924 (2018).
[22] M. M. Ugeda, A. J. Bradley, Y. Zhang, S. Onishi, Y. Chen, W. Ruan, C. Ojeda-Aristizabal, H. Ryu, M. T. Edmonds, H.-Z. Tsai, A. Riss, S.-K. Mo, D. Lee, A. Zettl, Z. Hussain, Z.-X. Shen, and M. Crommie, Nat. Phys. **12**, 92 (2016).
[23] R. Bianco, L. Monacelli, M. Calandra, F. Mauri, and I. Errea, Physical Review Letters **125**, 106101 (2020).
[24] M. Leroux, I. Errea, M. Le Tacon, S.-M. Souliou, G. Garbarino, L. Cario, A. Bosak, F. Mauri, M. Calandra, and P. Rodière, Phys. Rev. B **92**, 140303 (2015).
[25] K. Cho, M. Kończykowski, S. Teknowijoyo, M. A. Tanatar, J. Guss, P. Gartin, J. M. Wilde, A. Kreyssig, R. McQueeney, A. I. Goldman, *et al.*, Nat. Comm. **9**, 1 (2018).
[26] H. Wang, X. Huang, J. Lin, J. Cui, Y. Chen, C. Zhu, F. Liu, Q. Zeng, J. Zhou, P. Yu, *et al.*, Nat. Comm. **8**, 1 (2017).
[27] D. Wickramaratne, M. Haim, M. Khodas, and I. I. Mazin, Phys. Rev. B **104**, L060501 (2021).
[28] J. Bekaert, E. Khestanova, D. G. Hopkinson, J. Birkbeck, N. Clark, M. Zhu, D. A. Bandurin, R. Gorbachev, S. Fairclough, Y. Zou, *et al.*, Nano letters **20**, 3808 (2020).
[29] S. Divilov, W. Wan, P. Dreher, E. Bölen, D. Sánchez-Portal, M. M. Ugeda, and F. Ynduráin, Journal of Physics: Condensed Matter **33**, 295804 (2021).
[30] S. Das and I. I. Mazin, Comput. Mater. Sci. **200**, 110758 (2021).
[31] W. Wan, P. Dreher, R. Harsh, F. Guinea, and M. M. Ugeda, arXiv preprint arXiv:2101.04050 (2021).
[32] A. A. Abrikosov and L. P. Gor'kov, Zhur. Eksptl'. i Teoret. Fiz. **39** (1960).
[33] E. Margine and et. al., "In preparation".
[34] O. V. Dolgov, I. I. Mazin, A. A. Golubov, S. Y. Savrasov, and E. G. Maksimov, Phys. Rev. Lett. **95**, 257003 (2005).
[35] C. Heil, S. Poncé, H. Lambert, M. Schlipf, E. R. Margine, and F. Giustino, Phys. Rev. Lett **119**, 087003 (2017).
[36] A. Anikin, R. D. Schaller, G. P. Wiederrecht, E. R. Margine, I. I. Mazin, and G. Karapetrov, Phys. Rev. B **102**, 205139 (2020).
[37] M. M. Ugeda, "Private communication".
[38] J. Peng, Z. Yu, J. Wu, Y. Zhou, Y. Guo, Z. Li, J. Zhao, C. Wu, and Y. Xie, ACS nano **12**, 9461 (2018).
[39] L. Li, X. Deng, Z. Wang, Y. Liu, M. Abeykoon, E. Dooryhee, A. Tomic, Y. Huang, J. B. Warren, E. S. Bozin, *et al.*, npj Quantum Materials **2**, 1 (2017).
[40] H. Luo, W. Xie, J. Tao, H. Inoue, A. Gyenis, J. W. Krizan, A. Yazdani, Y. Zhu, and R. J. Cava, Proceedings of the National Academy of Sciences **112**, E1174 (2015).
[41] P. E. Blöchl, Phys. Rev. B **50**, 17953 (1994).
[42] G. Kresse and J. Hafner, Phys. Rev. B **47**, 558 (1993).
[43] G. Kresse and J. Furthmüller, Phys. Rev. B **54**, 11169 (1996).
[44] J. P. Perdew, K. Burke, and M. Ernzerhof, Phys. Rev. Lett. **77**, 3865 (1996).
[45] G. Henkelman and H. Jónsson, The Journal of chemical physics **113**, 9978 (2000).
[46] L. Sandratskii, Journal of Physics: Condensed Matter **3**, 8565 (1991).